

Three-dimensional numerical modelling of flow field in shallow reservoirs

Esmaeili, Sumi, Kantoush, Haun and R  ther

ice | proceedings

ICE Publishing: All rights reserved

Three-dimensional numerical modelling of flow field in shallow reservoirs

1 Taymaz Esmaeili MSc

PhD Student, Department of Urban Management, Graduate School of Engineering, Kyoto University, Kyoto, Japan

2 Tetsuya Sumi PhD

Professor, Disaster Prevention Research Institute (DPRI), Kyoto University, Kyoto, Japan

3 Sameh A Kantoush PhD

Associate Professor, Disaster Prevention Research Institute (DPRI), Kyoto University, Kyoto, Japan

4 Stefan Haun PhD

Scientific Assistant, Institute for Modelling Hydraulic and Environmental Systems, University of Stuttgart, Stuttgart, Germany

5 Nils R  ther PhD

Associate Professor, Department of Hydraulic and Environmental Engineering, Norwegian University of Science and Technology, Trondheim, Norway



Shallow flows can play a significant role in sediment management for dam reservoirs (e.g. sedimentation in shallow reservoirs and free-flow flushing operation). When shallow flow emerges with symmetric or asymmetric patterns, the flow domain exhibits complex three-dimensional (3D) features (e.g. helical flows). This study focuses on the numerical modelling of the velocity field in shallow reservoirs with varying geometries and also varying bed conditions (i.e. flat and misshaped beds). A fully 3D numerical model using the finite-volume method was utilised to reproduce the 3D flow velocity field. The experimentally measured surface velocity in all cases and velocity profiles in one case were used to validate the model. The numerical results showed that a slight disturbance in the inflow boundary condition results in a steady asymmetric flow pattern in reservoirs with a higher defined shape factor, but does not affect the flow pattern in reservoirs with a lower defined shape factor. Nonetheless, the simulated and measured flow velocity fields are reasonably consistent in all cases. These results can be used to optimise the design of sand traps or water storage facilities, and also to optimise sediment management in existing reservoirs.

Notation

B	reservoir width
b	inlet channel width
g	acceleration of gravity
h	flow depth
i	index for three spatial directions
k	turbulence kinetic energy
k_s	equivalent bed roughness
L	reservoir length
P	pressure
P_k	production of turbulent kinetic energy
Q	flow discharge
t	time
u	velocity fluctuations
u^*	shear velocity

U_i	averaged flow velocity in i direction
V_0	reference streamwise velocity at the inlet
V_{in}	actual streamwise velocity at the inlet, which is affected by a slight disturbance
x	coordinate in longitudinal direction
x_i	spatial geometric scale
y	coordinate in transversal direction
z	coordinate in vertical direction
α	magnitude of linear variation of streamwise velocity along the inlet channel width
δ_{ij}	Kronecker delta
ε	dissipation of k
ν	viscosity of water
ν_t	eddy viscosity
ρ	density of water

1. Introduction

Shallow flows are described as a flow condition in which the vertical dimension of the fluid domain is noticeably smaller than its horizontal dimensions (Yuce and Chen, 2003). Flows in wide rivers, lakes, coastal lagoons, estuaries and large reservoirs are examples of shallow waters in the prototype scale. A flow pattern in wide and shallow reservoirs with a sudden expansion of the inlet section may become unstable, which produces large-scale transversal motions and recirculation zones. This phenomenon can be attributed to the high sensitivity of the flow pattern to the initial boundary condition at the inlet section (e.g. small transverse disturbance) (Dewals *et al.*, 2008). When large-scale transverse motions and turbulent coherent structures develop in a shallow reservoir, the sediment transportation pattern (i.e. erosion and deposition) is significantly affected by the velocity field.

Shallow flows are predominant in nature and also emerge in many engineering applications such as sudden expansions (Shapira *et al.*, 1990), compound channels (Chu *et al.*, 1991; Ghidaoui and Kolyshkin, 1999), storage chambers (Adamson *et al.*, 2003; Stovin and Saul, 1996), settling tanks (Frey *et al.*, 1993), shallow reservoirs sedimentation (Camnasio *et al.*, 2013; Dufresne *et al.*, 2012; Kantoush *et al.*, 2008a, 2010) and sediment flushing (Esmaeili *et al.*, 2014b; Kantoush and Schleiss, 2009).

The effect of geometric and hydraulic boundary conditions on the flow pattern of shallow reservoirs was clarified in the experimental tests of Dufresne *et al.* (2011) and Kantoush (2008). Kantoush (2008) presented a comprehensive review of experimental tests in a series of shallow reservoirs with transverse flow motions in the symmetric channel expansions. His study revealed three-dimensional (3D) features of the flow structure in shallow reservoirs (i.e. secondary flows and 3D stretching vortices). In addition, the experimental tests show that an asymmetric flow pattern emerges under a certain geometric and hydraulic condition despite the perfect symmetric geometry and hydraulic condition. Similar results were obtained by Adamson *et al.* (2003) and Stovin and Saul (1996) regarding storage chambers and storage tank sedimentation, respectively. Kolyshkin and Ghidaoui (2003) came to a similar conclusion about the development of an asymmetric flow pattern in the wake flows, and Mariotti *et al.* (2013) also presented the analysis of flow instabilities in the river mouth zone with a small width-to-depth ratio. Recently, Peltier *et al.* (2014a) presented a review of the experiments regarding shallow reservoirs, and suggested the domains for existence of varying flow patterns, including meandering flows, in shallow reservoirs (Peltier *et al.*, 2014b).

Dewals *et al.* (2008), Dufresne *et al.* (2011) and recently Peltier *et al.* (2014c) used two-dimensional (2D) numerical models to investigate the turbulent flow patterns in rectangular shallow

reservoirs. Their studies revealed that 2D depth-averaged numerical models can reasonably reproduce the flow velocity pattern in shallow rectangular reservoirs. As long as secondary current effects and velocity variations over the flow depth are not significant, 2D models can be utilised. Compared to 3D models that need a careful setting, 2D models benefit from a simpler setting. However, the geometry condition may be more complex in practical cases, and a complex 3D flow pattern can emerge. The 2D numerical models cannot simulate the secondary current effects directly, particularly velocity variations over the flow depth on misshaped beds of shallow reservoirs. Stansby (2006) concluded that 2D depth-averaged models could not consider the flow curvature over the bed friction that emerged because of the vertical mixing, which is induced by horizontal strain rates. This inability may lead into a significant underestimation of the bed friction in some cases. The complexity of 3D flow patterns is further magnified over the existing bed forms, on the misshaped bed, that is obtained after flushing and lowering the water level. Because completely different flow patterns may appear over the flow depth, knowledge about the vertical distribution of the streamwise and lateral velocity, which is reproduced using 3D numerical simulations, can provide a more precise evaluation of morphological processes in shallow reservoirs. Nonetheless, 3D numerical modelling of the symmetric and asymmetric turbulent flow fields in shallow reservoirs with varying geometries is scarce (Esmaeili *et al.*, 2014a).

A computational fluid dynamic (CFD) code called SSIIM (simulation of sediment movements in water intakes with multiblock option) was used in this study to simulate the 3D flow velocity field. The SSIIM program, which was developed at the Norwegian University of Science and Technology (NTNU), implements a 3D numerical model of flow field by solving the mass and momentum conservation equation in three dimensions using various turbulence closure approaches. Further modifications are also possible in several parts of the source code (Olsen, 2013). SSIIM was successfully applied to model the 3D flow field in open channels with large roughness elements (Fischer-Antze *et al.*, 2001), compound channels (Wilson *et al.*, 2003) and meandering channels (Stoesser *et al.*, 2010). SSIIM was also used for the coupled computation of flow and sediment fields in the physical model and prototype scale studies (e.g. Dehghani *et al.*, 2012; Esmaeili *et al.*, 2013; Fischer-Antze *et al.*, 2008; Olsen and Kjellesvig, 1999; Ruether *et al.*, 2005). Recently, this CFD code with enhanced features of grid generation was used to simulate sedimentation and flushing channel evolution in shallow reservoirs (e.g. Esmaeili *et al.*, 2014b; Harb *et al.*, 2014; Haun and Olsen, 2012a, 2012b).

The assessment of the flow field is necessary to characterise the domain of the main jet flow, reverse flow and eddies in a shallow reservoir. Knowledge about shallow flows leads to a more appropriate design of storage facilities (e.g. storage

tanks; sewer detention tanks) and more efficient sediment management strategies in reservoirs and settling basins (Kantoush *et al.*, 2011a, 2011b). Moreover, in a shallow reservoir with misshaped bed, the variation in flow velocity over the flow depth is noticeable due to the existing friction of the bed forms. However, a few studies have considered the effect of various geometric and hydraulic parameters on the flow pattern of shallow reservoirs. Consequently, 3D modelling of the velocity field on flat and misshaped beds of shallow reservoirs, without a sediment transport condition, was performed in this study and compared with the experimental measurements.

2. Physical model set-up and study cases

The experimental tests were performed at the Laboratory of Hydraulic Constructions of the Swiss Federal Institute of Technology (EPFL) in a rectangular reservoir with a maximum inner length (L) of 6 m and width (B) of 4 m (Kantoush, 2007). The inlet and outlet rectangular channel width (b) and length (l) were 0.25 m and 1 m respectively. Both channels were located at the centre of the upstream and downstream side walls of the reservoir. Various shallow reservoir geometries could be achieved by adjusting a moveable polyvinyl chloride (PVC) plate wall. The reservoir depth was 0.3 m, and both side walls and the bottom floor were hydraulically smooth and flat. The water level in the reservoir was controlled using a 0.25 m wide and 0.3 m high flap gate at the end of the outlet channel. A movable frame of 4 m length was mounted on the side walls of the reservoir to install the measurement devices. Table 1 shows the geometrical attributes of five reservoirs used in the present study and also corresponding shape factors (i.e. SF) described by Dufresne *et al.* (2011). According to Dufresne *et al.* (2011), the flow pattern was symmetric (i.e. S0) when SF was approximately lower than 6.2 and the flow pattern was asymmetric (i.e. A1) when SF was approximately bigger than 6.8. Thus, in the applied geometries, T11 and T13 have S0 flow pattern whereas T7, T8 and T9 have A1 flow pattern.

Case	b : m	l : m	B : m	ΔB^a	SF ^b
T7	0.25	6	3	1.375	8.63
T8	0.25	6	2	0.875	11.32
T9	0.25	6	1	0.375	18.82
T11	0.25	5	4	1.875	5.97
T13	0.25	3	4	1.875	3.58

^a ΔB is equal to $(B - b)/2$

^bSF is the shape factor introduced by Dufresne *et al.* (2011), which is defined as $L/\Delta B^{0.6} b^{0.4}$

Table 1. Geometrical attributes of experimental cases employed by Kantoush (2008)

The large-scale particle image velocimetry (LSPIV) technique was used to measure the surface velocity field, and ultrasonic velocity profiler (UVP) devices were used to provide the 3D flow velocity measurements (Kantoush *et al.*, 2008b). Each UVP device can instantaneously measure 1D velocity profile over the flow depth. A set of three UVP probes, which were inclined at 20° to the vertical axis and installed on the movable frame, allowed measurement of the 3D flow field. The first valid UVP measurements were located 12.5 cm away from the side walls and 2.5 cm from the free water surface. Additionally, in the framework of the experimental study, the surface velocity was measured after sediment flushing from the shallow reservoirs. Plastic particles with a density of 960 kg/m³ and an average diameter of 3.4 mm were used as seed for LSPIV measurements (Kantoush *et al.*, 2008b). Non-uniform crushed walnut shells were used as fluid tracers to provide ultrasound reflection for UVP devices and were also used as suspended material for modelling sediment deposition. The median size of this non-cohesive lightweight and homogenous grain material was 50 µm with a density of 1500 kg/m³. The flow discharge rate (Q) and water depth (h) were fixed for all experiments as 0.007 m³/s and 0.2 m respectively, except for the cases with a misshaped bed. Thus, in all examined configurations with a flat bed, the measured Froude number was as small as $Fr = 0.1$ and Reynolds number was as high as $14\,000 \leq Re \leq 28\,000$ to ensure that a turbulent flow was developed. For the flow field measurements on misshaped beds after flushing, the water level and discharge were 0.1 m and 0.007 m³/s respectively.

Five different reservoir geometries with various length-to-width (aspect) ratios and reservoir width to inlet channel width (expansion) ratios used in the experimental study of Kantoush (2007) were considered to numerically model the different flow patterns encountered. The hydrodynamic boundary utilised in the experimental work was also employed. The flat bed and misshaped bed, which were obtained after flushing and lowering the water head, were introduced to the SSIIM program as the initial bed condition. The numerical results were compared and validated with a 2D systematic measured surface velocity, which was provided using the LSPIV technique for all cases. Additionally, simulated 3D velocity components were compared with the measured values, which were obtained using UVP devices in one case.

3. Numerical model

The fully 3D numerical model SSIIM used in this study solves the continuity equation together with Reynolds-averaged Navier–Stokes equations in a 3D grid to compute the water motion for turbulent flows (Olsen, 2013)

$$1. \quad \frac{\partial U_i}{\partial x_i} = 0$$

$$2. \quad \frac{\partial U_i}{\partial t} + U_j \frac{\partial U_i}{\partial x_j} = \frac{1}{\rho} \frac{\partial}{\partial x_j} (-P \delta_{ij} - \rho \overline{u_i u_j})$$

where $i=1, 2, 3$ is representative of three directions; where U_j is the averaged flow velocity, x_i is the spatial geometrical scale, ρ is the water density, P is the Reynolds-averaged pressure, δ_{ij} is the Kronecker delta, and $-\rho \overline{u_i u_j}$ is the Reynolds stress term. The unknown pressure field in the Reynolds-averaged Navier–Stokes equations is calculated employing the semi-implicit method for pressure-linked equations (i.e. Simple method) (Patankar, 1980). The finite-volume approach is applied as a discretisation method to transform the partial equations into algebraic equations. The convection term in the Navier–Stokes equation is solved using the second-order upwind scheme. The Reynolds stress term is modelled using the standard $k-\varepsilon$ turbulence model with constant empirical values (Lauder and Spalding, 1972)

$$3. \quad -\overline{u_i u_j} = \nu_t \left(\frac{\partial U_i}{\partial x_j} + \frac{\partial U_j}{\partial x_i} \right) - \frac{2}{3} k \delta_{ij}$$

$$4. \quad \nu_t = \frac{c_\mu k^2}{\varepsilon}$$

where ν_t is the turbulent eddy-viscosity, k is the turbulent kinetic energy and ε is the dissipation rate of k . The equations for k and ε are as follows

$$5. \quad \frac{Dk}{Dt} = \frac{\partial k}{\partial t} + U_j \frac{\partial k}{\partial x_j} = \frac{\partial}{\partial x_j} \left[\left(\nu + \frac{\nu_t}{\sigma_k} \right) \frac{\partial k}{\partial x_j} \right] + P_k - \varepsilon$$

$$6. \quad \frac{D\varepsilon}{Dt} = \frac{\partial \varepsilon}{\partial t} + U_j \frac{\partial \varepsilon}{\partial x_j} = \frac{\partial}{\partial x_j} \left[\left(\nu + \frac{\nu_t}{\sigma_\varepsilon} \right) \frac{\partial \varepsilon}{\partial x_j} \right] + c_{1\varepsilon} \frac{\varepsilon}{k} P_k - c_{2\varepsilon} \frac{\varepsilon^2}{k}$$

where c_μ , $c_{1\varepsilon}$, $c_{2\varepsilon}$, σ_k and σ_ε are the constant empirical values and P_k denotes the production of kinetic energy

$$7. \quad P_k = \nu_t \frac{\partial U_i}{\partial x_j} \left(\frac{\partial U_j}{\partial x_i} + \frac{\partial U_i}{\partial x_j} \right)$$

The change in water levels was based on the calculated pressure field using the Simple method. The pressure was extrapolated to the water surface, and the pressure difference between a surface node and a downstream node was used to estimate the water elevation difference (Olsen, 2013). This

iterative approach is stable and has been used successfully for simulating a complex flow pattern in a number of cases such as the Danube river (Tritthart and Gutknecht, 2007). The grid is adaptive and moves with the changes of the bed and water levels.

The Dirichlet boundary condition for the water inflow (logarithmic velocity distribution) was used, whereas the zero-gradient boundary condition was specified for the water outflow. For rough boundaries of the side walls and the bed, where there is no water flux, the empirical wall laws introduced by Schlichting (1979) were utilised. For smooth boundaries, other wall law functions were used (Olsen, 2013).

Based on the grid that was used for experimental measurements, the computational mesh for all reservoir geometries was made. The mesh cell size for the cases T7, T8, T9, T11 and T13 in the X and Y directions was $5 \text{ cm} \times 2.5 \text{ cm}$, $5 \text{ cm} \times 2.5 \text{ cm}$, $5 \text{ cm} \times 2.5 \text{ cm}$, $5 \text{ cm} \times 2 \text{ cm}$ and $2.5 \text{ cm} \times 1 \text{ cm}$, respectively. Considering 11 cells for the vertical grid distribution, the total number of cells over the main reservoir geometry was 158 400, 107 360, 52 800, 220 000 and 528 000. Due to the sensitivity of the flow pattern in case T13, a mesh with a higher resolution was used, which was equal to $2.5 \text{ cm} \times 1 \text{ cm}$.

4. Simulation results and discussions

4.1 Surface velocity field on flat beds

Kantoush (2008) observed that in case T7 the issuing flow jet deviated to the right-hand side and developed an A1 flow pattern. The main eddy rotated anticlockwise in the centre part of the reservoir, and two smaller eddies rotated clockwise in the upstream corners. Additionally, a S0 flow pattern with one main jet trajectory in the centreline and two circulation zones on each side was developed for case T13. Kantoush (2007) concluded that the deviation to the right-hand side occurred because of random disturbance of the initial flow boundary condition, and a symmetric situation would be easily established by slightly disturbing the initial boundary condition. The flow deflection to one side of the reservoir can be attributed to the difference in flow velocity along one side of the main jet compared with the other side, and the consequential pressure difference. The local pressure difference deviates the flow towards one side of the reservoir and is called the Coanda effect (Chiang *et al.*, 2000).

In the numerical simulation, the time step was set as 2 s for runs T8 and T9, whereas it was 0.5 s for T7, T11 and T13. Smaller time steps contributed to faster and more stable convergence of the computations in wider reservoirs. Simulations were performed using geometry and inflow/outflow boundary conditions that were similar to the physical model. The $k-\varepsilon$ turbulence model was used, and simulations were conducted until a steady-state flow condition was obtained. The

simulations show that the model cannot reproduce an A1 flow pattern when the geometry configuration and hydraulic boundary condition are perfectly symmetric because the applied mathematical algorithms were not intended to reproduce this type of artificial asymmetric numerical result when the input boundary condition is symmetric.

Because the S0 flow pattern was not observed in the physical model experiments for special geometries, Dewals *et al.* (2008) introduced a slight disturbance in the initial boundary condition for 2D numerical simulations. They used a non-uniform cross-sectional discharge in the inlet boundary to examine the stability of the numerical model outputs. The identical concept of slight disturbance in the inflow boundary condition was implemented here for all runs, and the non-uniform cross-sectional velocity distribution was used in the inflow boundary condition:

$$8. \quad V_{in}(x) = V_0 \left[1 - \alpha \left(0.5 + \frac{y}{b} \right) \right]$$

where V_{in} is the actual streamwise velocity value, which is specified as the inflow boundary condition, V_0 is the reference value (i.e. total discharge divided by inlet cross section area), α measures the magnitude of the linear variation, b denotes the inlet channel breadth and y is the coordinate along the transversal direction, which changes between $-b/2$ and $b/2$ (i.e. the right and left sides of the inlet channel respectively). Assuming that $\alpha = 2.5\%$ for numerical modelling, the initial velocity magnitude differs by 2.5% at one side of the inlet channel compared to the other side. This type of disturbance is inevitable in the experimental set-up. Nonetheless, a notably small perturbation of the inflow condition will significantly affect the A1 flow pattern in the numerical results. Changing α between 1 and 4% shows a notably close flow field to that observed in the physical model except for case T7, in which there is a threshold value for α . For this case, the smallest value of α to reproduce the A1 flow pattern is 2.5%, and this value is also used for other cases with A1 flow patterns. This type of result reveals the unstable nature of symmetric flows in such geometries, and consequently the high sensitivity of the flow field to the inflow boundary condition. Depending on which side of the inlet has the higher velocity, the jet deflection to each side of the reservoir (i.e. right or left) can be obtained. A limited number of runs also showed the contribution of the bed and side-wall roughness in the development of the A1 flow pattern in case T7 even with α of 1% when the roughness increases. A higher roughness can affect the initial flow condition, which is consistent with the findings of Chu *et al.* (1991) about the effect of friction on the velocity profile and consequently the flow pattern. However, an intensive numerical study should be performed in the future, with a physical model study on the interaction between slight disturbances in the inflow boundary condition and the side and bed roughness and their effect on the flow pattern.

Figure 1 shows the jet evolution pattern of case T7 after a jet was issued into the stagnant shallow water, which eventually established a steady asymmetric flow condition. First, when the main jet flow attaches to the downstream wall at $t = 240$ s, it returns backwards, which causes energy dissipation and velocity reduction as shown in Figure 1(a). Because of the non-uniform velocity distribution and the consequential pressure difference (Coanda effect), the flow field is transversally unstable, and the main jet flow slightly deviates to the left side. In the subsequent stage of $t = 240$ –480 s, a transitional

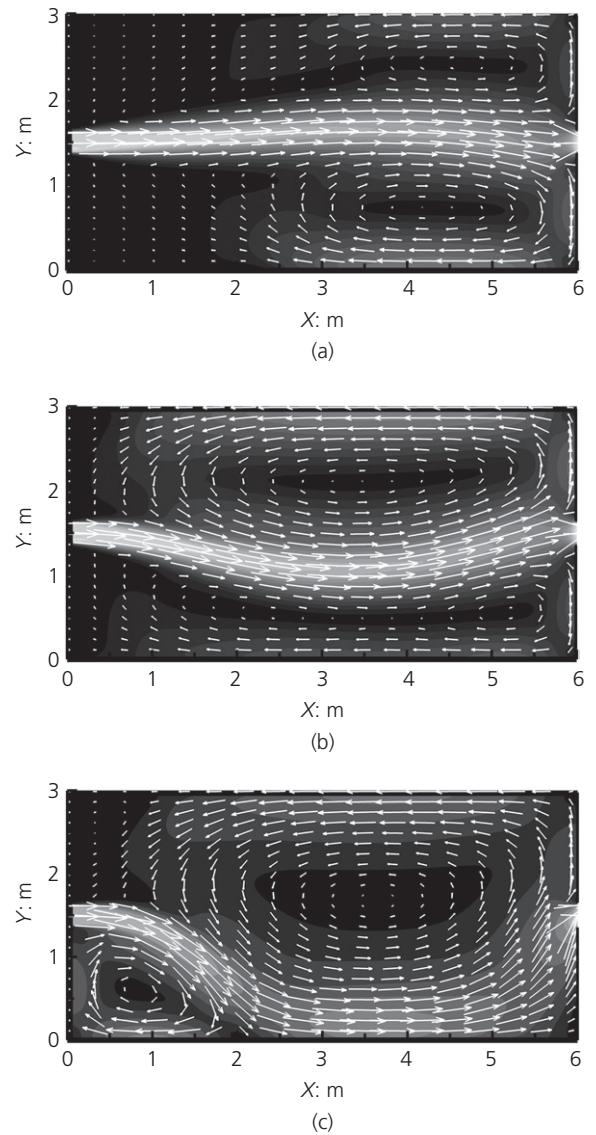


Figure 1. Various stages of asymmetric flow pattern development in shallow reservoirs with flat beds: (a) attachment of main jet flow to the downstream wall ($t = 240$ s); (b) deviation of main jet flow from centerline to the right-hand side during the transitional stage ($t = 480$ s) and (c) attachment of main jet flow to the right side wall ($t = 1800$ s)

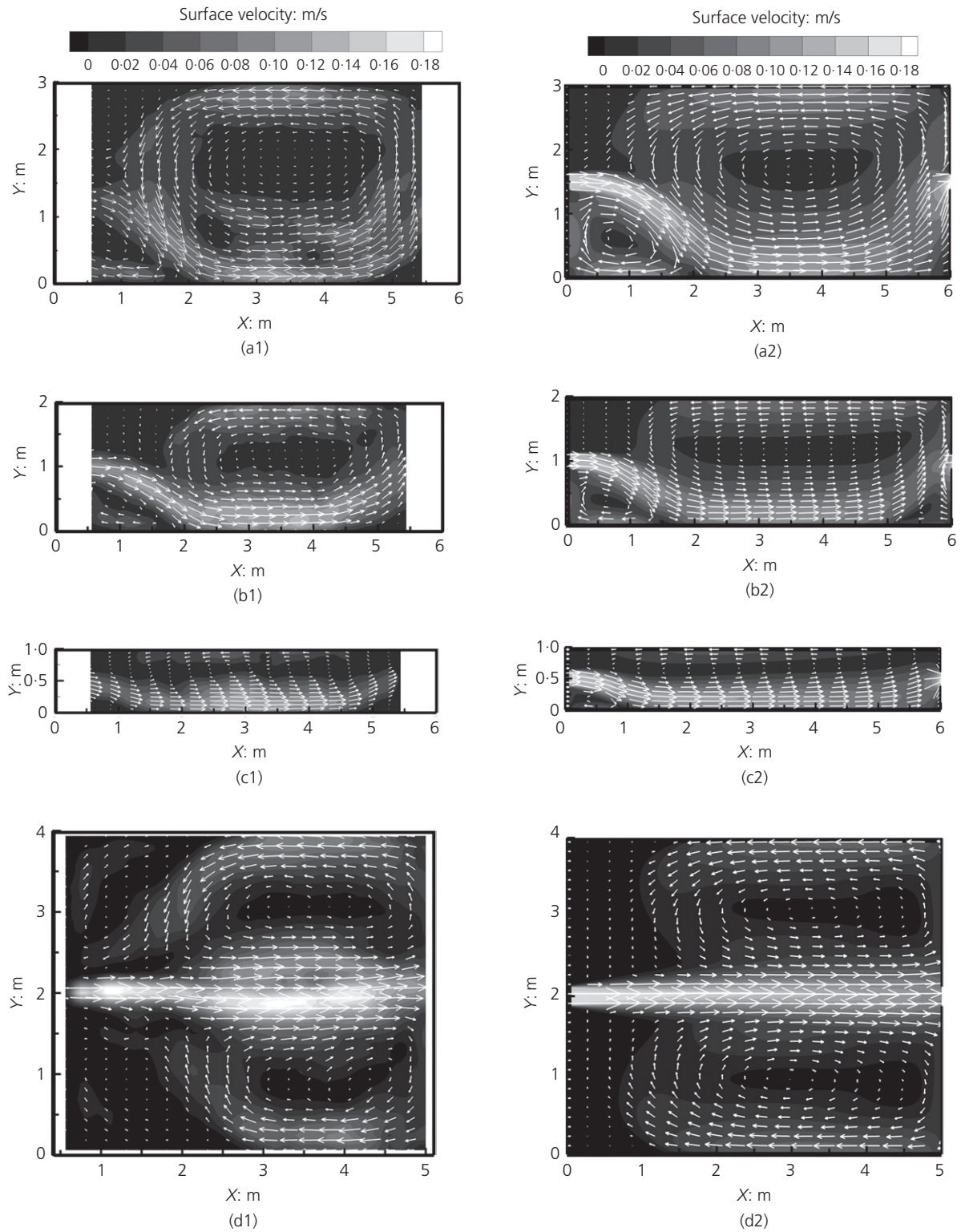


Figure 2. Left: the measured surface velocity field with velocity vectors over flat bed for case: (a1) T7; (b1) T8; (c1) T9; (d1) T11; (e1) T13, respectively and right: corresponding simulated velocity field for each case (continued on next page)

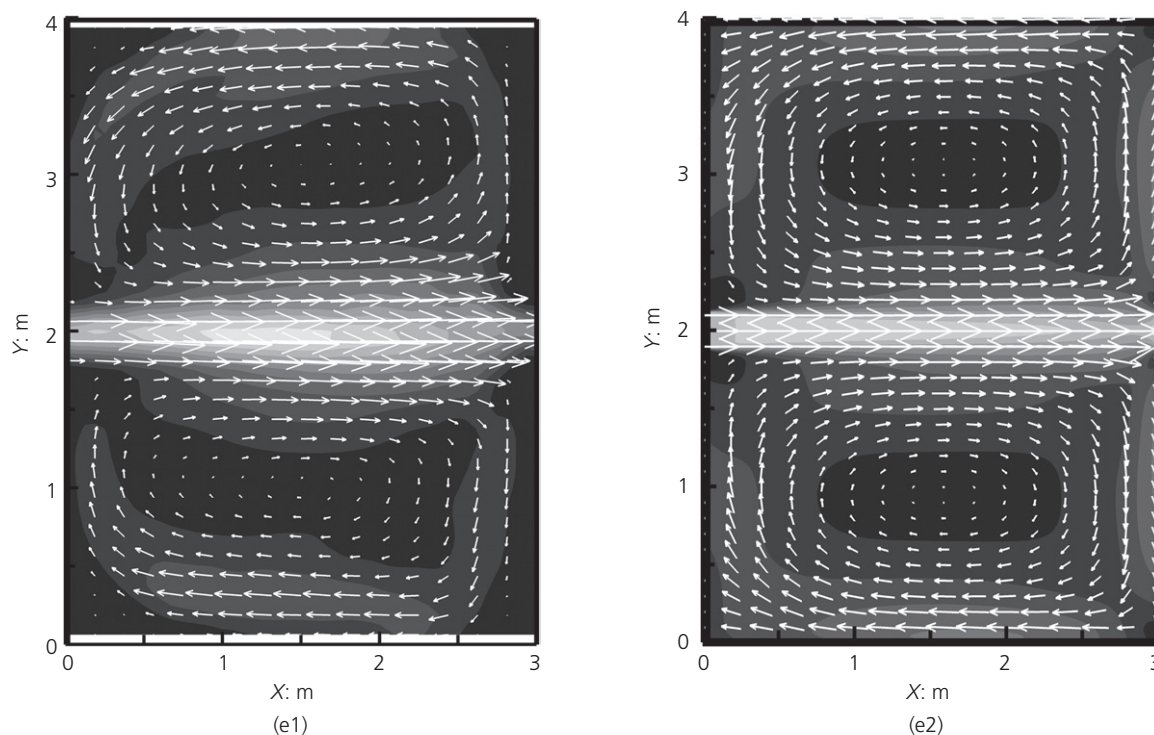


Fig. 2. Continued

phase occurs, where the jet gradually deviates from the left side to the right side as shown in Figure 1(b). Similar to the first stage, the locally reduced pressure because of the higher velocity on one side than the other side tends to amplify the jet deflection. Meanwhile, upstream corner vortices are formed and their size increases, which controls the centre anti-clockwise vortex. Afterwards, the main jet flow reattaches to the right side wall, and a steady A1 flow pattern finally emerges over the shallow reservoir as illustrated in Figure 1(c). The simulated jet evolution pattern was consistent with the experimental observations. Furthermore, an identical jet evolution pattern was obtained for cases T8 and T9.

Figure 2 illustrates the measured and simulated surface velocity magnitudes and flow distribution patterns for five selected experiments. As shown in Figure 2, an A1 flow pattern develops in cases T7, T8 and T9, whereas an almost S0 flow pattern develops in cases T11 and T13. The model can simulate a surface flow velocity pattern that is similar to the measured pattern by reproducing the dominant aspects of the flow field, such as the main flow jet trajectory, location of the reverse flow, main vortices and corner gyres. Nevertheless, the numerical model results show a straighter and longer reverse flow trajectory than the observations, and a concentrated main jet flow for all cases. Consequently, the upstream corner gyres in the numerical outputs have a smaller size than those of the experimental measurements. This situation is predominant for T11 (Figures 2(d1) and 2(d2)).

Figure 3 quantitatively demonstrates the simulated streamwise and transversal surface velocity distribution against the measured one at the middle cross-section of the reservoirs for cases T8 and T13. The numerical model results are consistent with the measurements in case T8, which has an A1 flow pattern as shown in Figure 3(a). Figure 3(b) shows that in case T13 there is a slight discrepancy between the simulated and measured surface velocity fields, particularly along the centre-line and side walls of the reservoir. The reason could be the concentrated simulated flow pattern, with a lower diffusion of the main jet and reverse jet flows compared to the measurements. Furthermore, Figure 4 shows similar outputs in both the upstream and downstream areas of case T7. The overall trend of surface velocity variations was reproduced using the numerical model. To provide a higher resolution longitudinal distribution of the surface velocity, the simulated streamwise velocity along the reservoir length (i.e. beside the right wall, along the centre-line and beside the left wall) was plotted against the measured velocity for case T8 and for the right half of case T13 in Figure 5. As shown in Figure 5(a), regarding case T8, apart from the area near the inlet and outlet, the numerical model results are reasonably consistent with the measurements. An identical condition was found for the other cases with A1 flow pattern (e.g. cases T7 and T9). The longitudinal velocity distribution for the left half of case T13, as depicted in Figure 5(b), is notably close to that of the right half. Figures 3–5 show that numerical results are globally consistent with the measured surface velocity components for varying geometries with varying flow patterns.

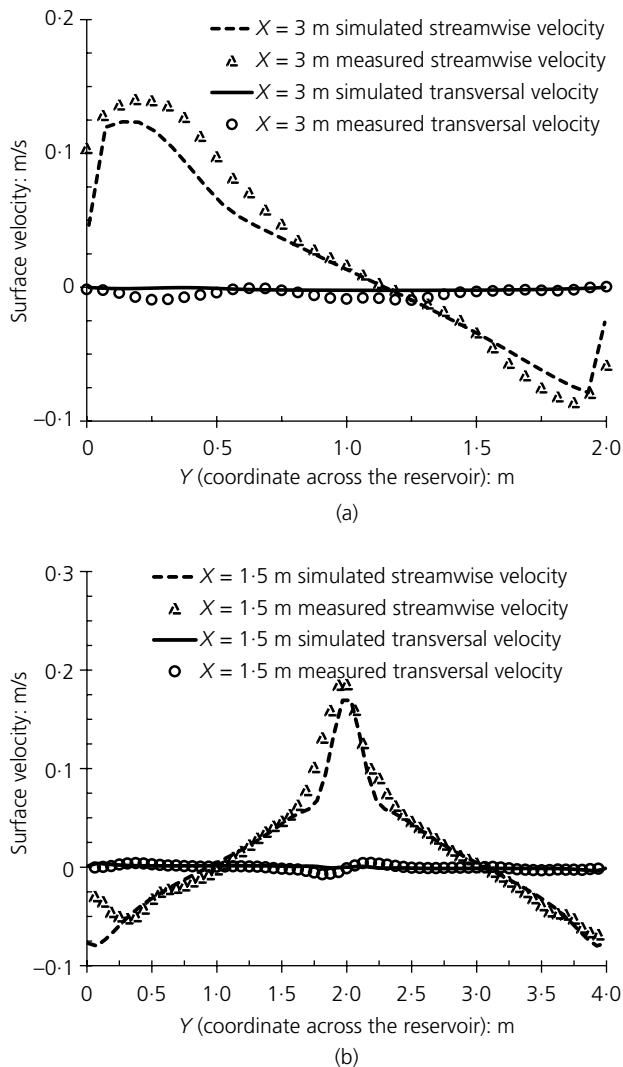


Figure 3. The measured streamwise and transversal surface velocity against the simulated velocity at the middle of the reservoirs' length with the flat bed condition for case: (a) T8; (b) T13; the view direction is upstream

It should be noted that there may be more than one solution for initiating the A1 flow pattern. Thus, other types of slight disturbances of the inlet boundary condition can produce the A1 flow pattern in relevant cases (e.g. slight deflection of the inlet channel or a combination of inlet channel deflection and non-uniform cross-sectional velocity).

4.2 Surface velocity field on misshaped beds

The measured bed morphology for cases T8, T11 and T13 after sediment flushing and lowering the water head is shown in Figure 6. The bed morphology was introduced to the model as the initial boundary condition for each case to simulate the 3D flow field. In addition, a slight disturbance of the inflow boundary condition was not considered. Because

of the shallower flow condition, with higher velocity components on the existing friction of various bed forms, the flow field simulation on misshaped beds is more complex than that on flat beds. For all three cases, the bed roughness was considered as 0.00015 m, which is three times the median grain size.

The measured surface velocity after flushing using the LSPIV technique and the simulated surface velocity using the 3D model are shown in Figure 7. For case T8, Figures 7(a1) and 7(a2) show that the simulated hydraulic and geometric features of the main jet flow and reverse flow trajectory are slightly different from the measured ones. Here, the developed flushing channel attracts the jet flow and stabilises the flow pattern. Similarly to the surface velocity pattern on flat beds, the reverse flow trajectory is longer and straighter, and the upstream vortices have smaller longitudinal size than the observed ones. The differences between the measured and simulated surface velocity patterns and sizes of the upstream vortices are more prominent in cases T11 and T13. Figures 7(b1) and 7(b2) show that the upstream corner vortices cannot be reproduced by the numerical model for case T11, while their sizes are underestimated in case T13, as shown in Figures 7(c1) and 7(c2). Compared to the flow patterns in shallow reservoirs with flat beds, there is more discrepancy between the simulation results and the measurements. One possible reason for this discrepancy is the presence of various types of bed forms with different roughness values at different places on the bed floor. Another reason is the $k - \epsilon$ turbulence model, which represents a lower diffusion in simulation of the flow field in shallow reservoirs (Dewals *et al.*, 2008).

The simulated streamwise and transversal surface velocities at the middle of the channel length were plotted against the measured velocities in Figure 8. Similar to the surface velocity field on flat beds, the numerical outputs are quantitatively in reasonable agreement with the measurements. Figure 9 also shows the simulated surface velocity against the measured velocity in the upstream and downstream zones of case T11. This figure shows a small deviation of the main jet flow from the centreline of the reservoir, which first goes to the right side (Figure 9(a)) and subsequently to the left-hand side (Figure 9(b)). This deviation implies a non-straightforward flow motion along the centreline when the reservoir is wide.

4.3 Velocity distribution over the flow depth

The velocity field distribution over the flow depth is important for analysing sediment transportation in reservoirs. The numerically simulated 3D flow velocity field in the reservoirs with flat beds was therefore compared with the measured 3D velocity components that were provided using the UVP measurements. Figure 10(a) shows the measured streamwise velocity distribution over the flow depth in upstream, middle, and downstream areas of case T8. Figure 10(b) corresponds to the simulated streamwise velocity for this case.

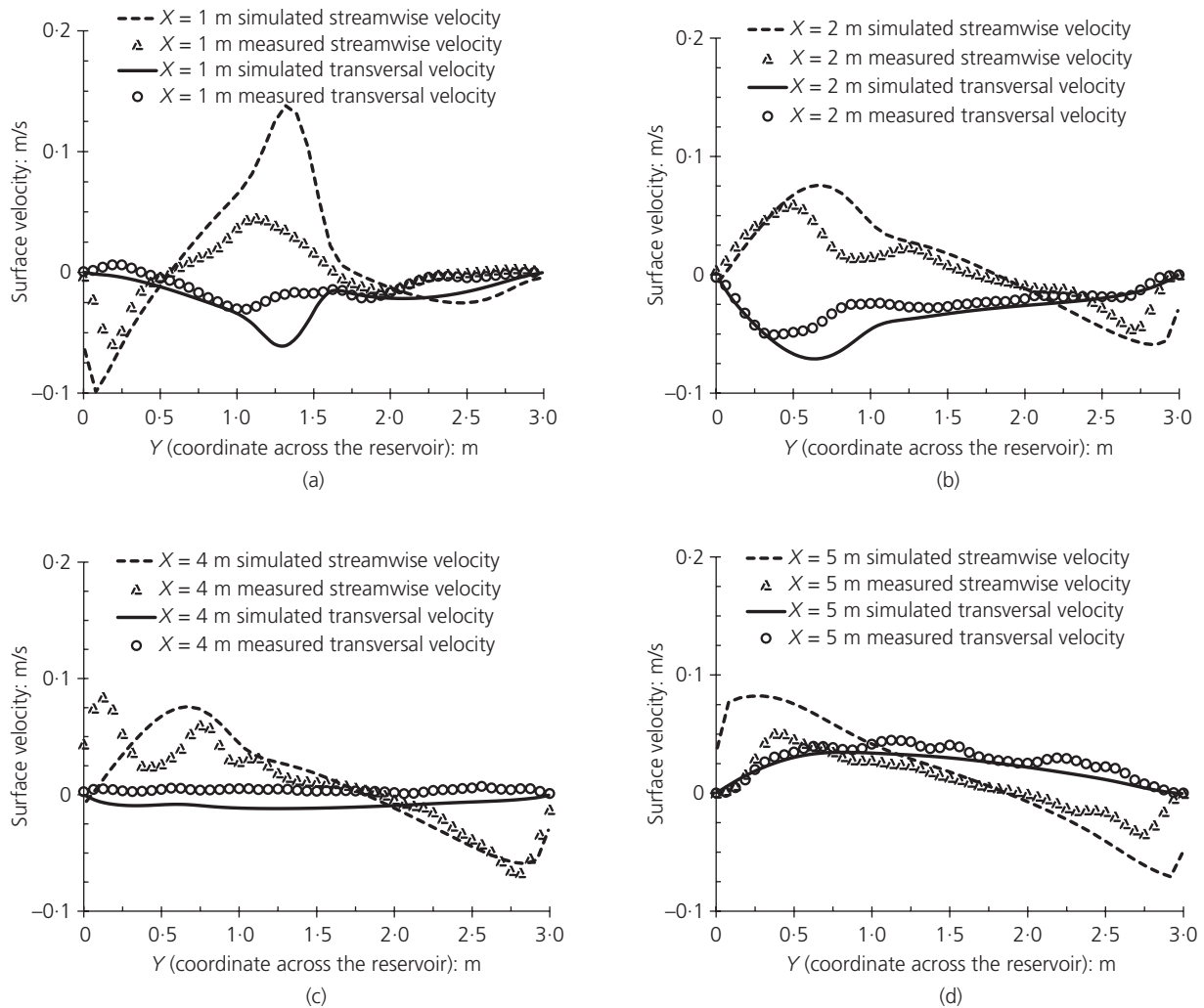


Figure 4. The measured streamwise and transversal surface velocity against the simulated one for case T7 at: (a) $x = 1$ m; (b) $x = 2$ m; (c) $x = 4$ m; (d) $x = 5$ m; the view direction is upstream

Regarding the cases with misshaped beds, the simulated lateral flow velocity contours over the depth and the secondary flow velocity vectors at the middle of the reservoir length are illustrated in Figures 10(c) and 10(d) for case T8 and the right half of case T13 respectively. Numerical outputs in Figure 10(b) reveal that higher longitudinal velocity is deflected towards the right bank side, and the reverse flow is reproduced near the left bank side. This change in flow direction across the reservoir is also qualitatively consistent with the experimental observations in Figure 10(a). The measurements also show that the vertical velocity magnitudes over the flow depth are notably small compared to the other velocity components (i.e. streamwise and lateral) when the reservoir bed is flat and horizontal. The discrepancy between the calculated and measured outputs can be attributed to the existing roughness of the side walls, which affects the flow field and was neglected in the

computations. On the other hand, Figures 10(c) and 10(d) show the complexity of the 3D flow field development on existing bed friction in shallow reservoirs with misshaped beds, where the velocity magnitude and direction can vary over the flow depth, and circulation zones in the vertical direction may emerge. This type of output is beneficial for a precise analysis of flow characteristics (e.g. water levels) and potential erosion and deposition zones during anticipated floods, when the bed has been disturbed and complex bed geometry has been developed because of the sediment flushing process.

To more comprehensively assess the numerical model results, the velocity field in the streamwise and lateral directions (i.e. U , V , respectively) at two different vertical levels from the bed (i.e. $z = 0.045$ m, 0.155 m), in three longitudinal sections for cases T8, is shown in Figure 11. This figure shows that

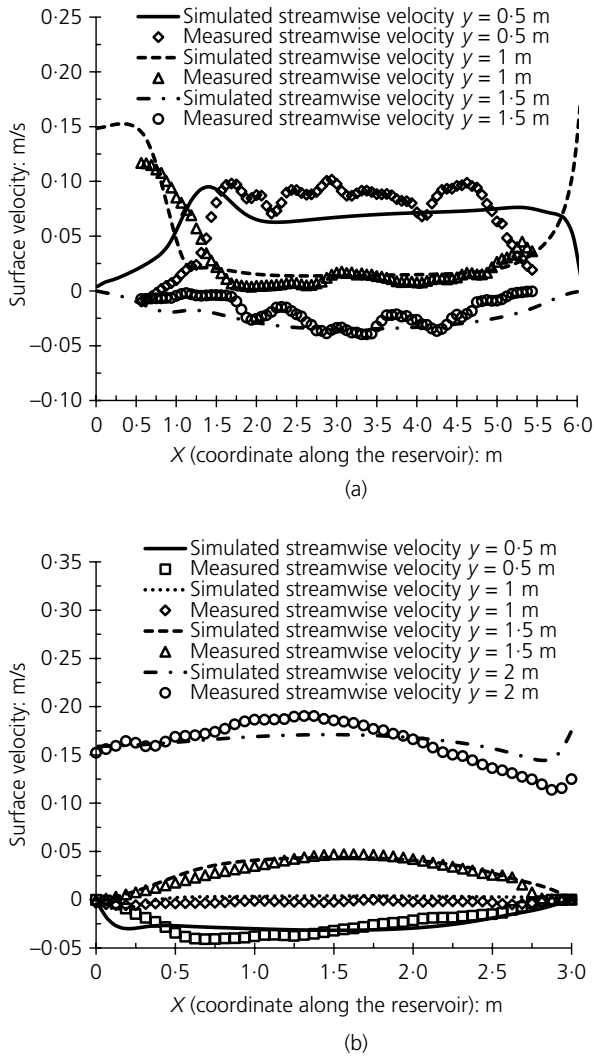


Figure 5. Longitudinal distribution of surface streamwise velocity over the flat bed reservoirs for: (a) case T8; (b) the right half of case T13

streamwise velocity magnitudes are different from the measured ones near the inlet, particularly at the level near the surface (i.e. $z=0.155$ m). This difference is considerable for the longitudinal section adjacent to the left side wall (i.e. $y=1.625$ m), because a complex combined vortex is formed at the upstream left zone of the reservoir consisting of two smaller sub-vortices with different rotation directions. It should be noted that the numerical model mainly reproduces one vortex system in this area. The simulated streamwise velocities are generally consistent with the UVP measurements in other parts of the reservoir, although some fluctuations are found in the measurements. Regarding the transversal velocities, the numerical model outputs are reasonably consistent with the measurements except in the aforementioned upstream zone. The numerical model outputs represent the negative transversal

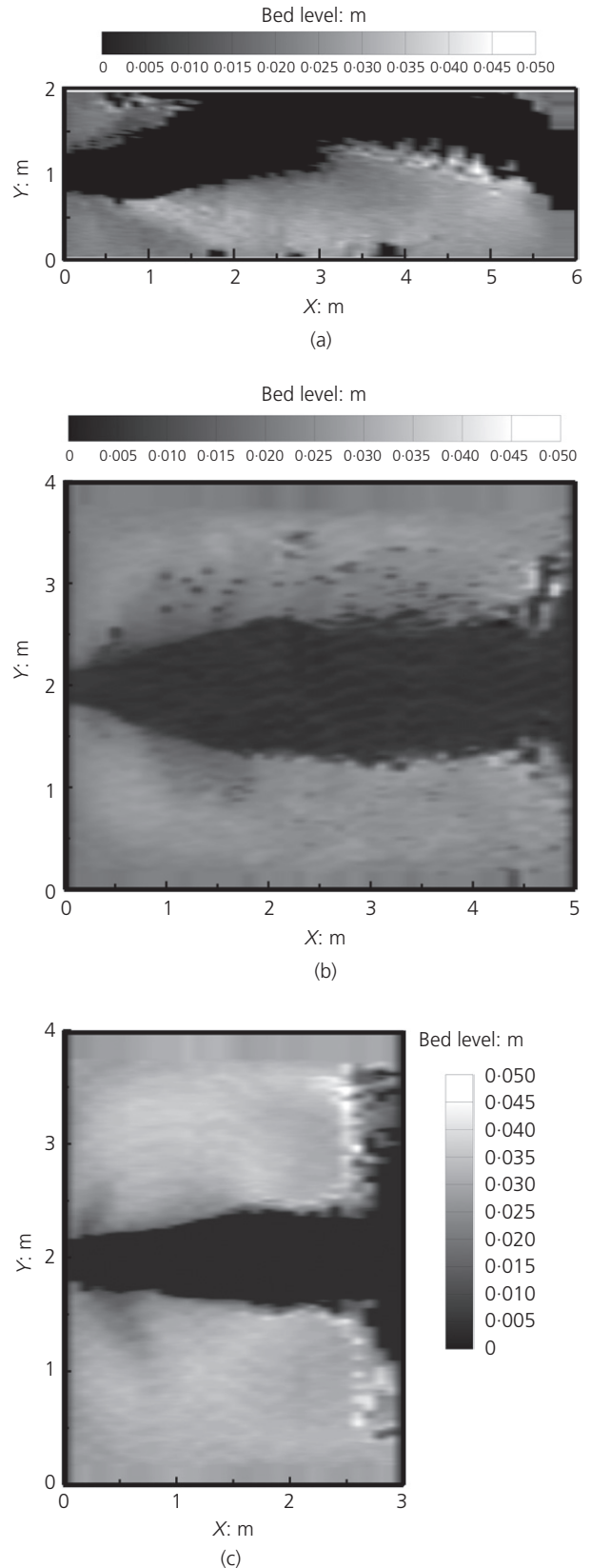


Figure 6. The misshaped bed obtained after sediment flushing with lowering the water level for case: (a) T8; (b) T11; (c) T13

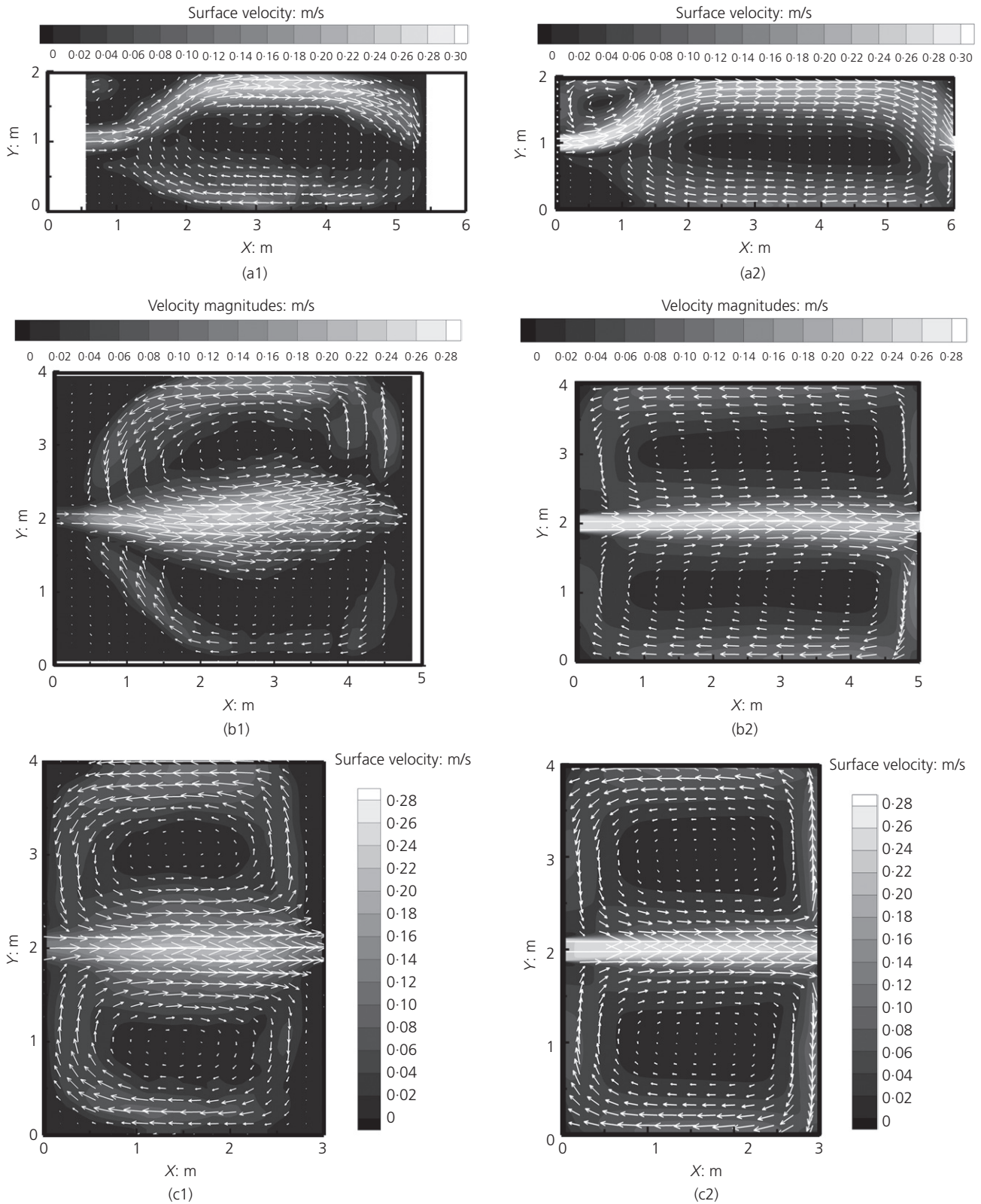


Figure 7. Left: the measured surface velocity field with vectors over misshaped bed after flushing for case: (a1) T8; (b1) T11; (c1) T13, respectively and right: corresponding simulated velocity field for each case

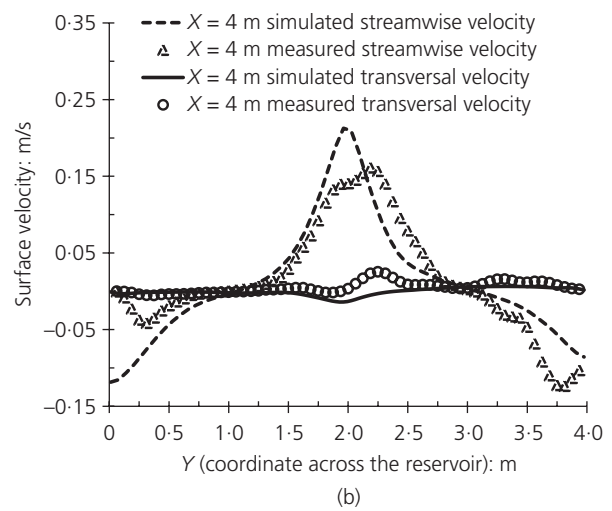
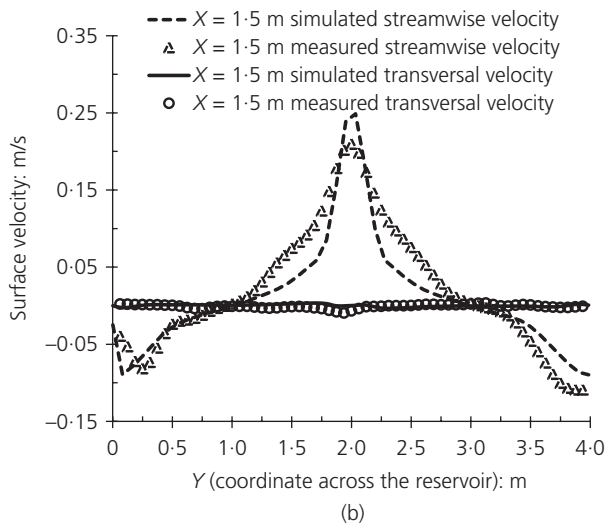
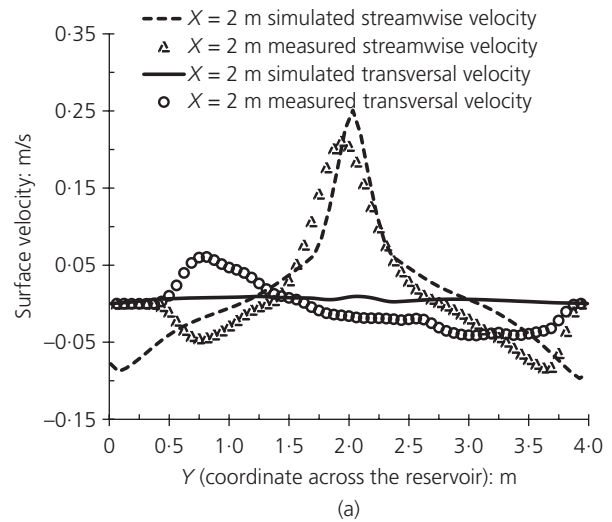
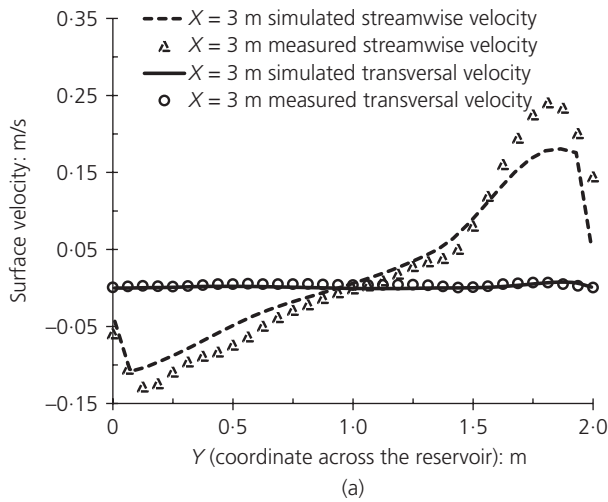


Figure 8. The measured streamwise and transversal surface velocity against the simulated one at the middle of the reservoirs' length with misshaped bed condition for case: (a) T8; (b) T13; the view direction is upstream

Figure 9. The measured and simulated surface velocity over the misshaped bed of case T11 at (a) $x=2$ m; (b) $x=4$ m; the view direction is upstream

velocities, whereas the measured velocities show positive values because of the existing complex combined vortex.

5. Conclusions

In the present study, the SSIIM program was used to reproduce the 3D velocity field on flat and misshaped beds of rectangular shallow reservoirs with varying geometries. The surface velocity was measured using the LSPIV technique to validate the model. In addition, 3D velocity components over the flow depth, which were provided by the UVP, were compared with the numerical results. The following results were obtained from the present work.

- Various aspects and hydrodynamic characteristics of shallow waters in varying reservoir geometries such as

jet trajectory, recirculation zones, eddies and flow distribution pattern, can be represented by the numerical model on both flat and misshaped beds. Two sets of hydraulic parameters (e.g. water depth, Froude number, roughness) corresponding to each bed type (i.e. flat or misshaped) were used in the simulations. Similarly to the observations, the model reproduces both symmetric (S0) and asymmetric (A1) flow patterns in the symmetric geometry set-up of the reservoirs after introducing a slight disturbance in the inflow boundary condition (i.e. perturbation) for all cases with a flat bed. The numerical results show that the flow pattern is insensitive to the small disturbance in the inflow boundary condition of the geometries with lower shape factors (i.e. cases T11 and T13). In this condition, the numerical model converges to a steady S0 flow pattern. However, the

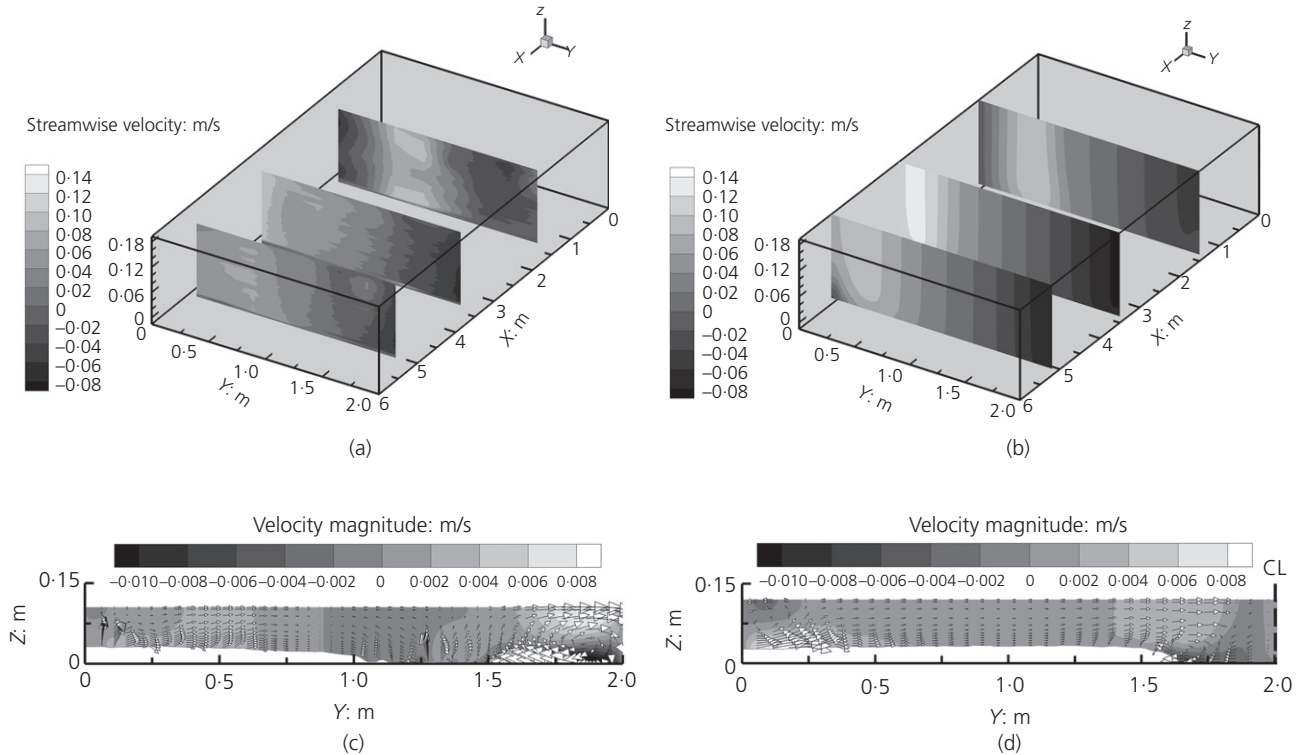


Figure 10. The streamwise velocity distribution over the flow depth of case T8 with flat bed at $x=1.5$ m, 3.5 m and 5.2 m using (a) UVP measurement and (b) 3D numerical model; simulated

lateral velocity distribution over the flow depth at $x=3$ m on misshaped bed of (c) T8 and (d) right half of T13

calculated flow pattern in geometries with higher shape factors (i.e. cases T7, T8 and T9) converges to a steady A1 flow pattern. Regardless of the bed condition, the computed flow velocity magnitudes are reasonably consistent with the experimental observations. Some discrepancy exists between the numerical results and the measurement in the upstream vortex dimensions and flow field in this area for both bed types. This discrepancy is mainly due to the simulated longer flow and reverse flow jet patterns, and also to the simulated concentrated flow and reverse flow jet patterns with a lower flow diffusion in the numerical outputs. The lower diffusion can be attributed to the application of the standard $k-\epsilon$ turbulence model. In the case of the misshaped beds, the varying bed friction over the reservoir geometry may increase the discrepancy.

- Further development of the study with higher Froude numbers (e.g. greater than 0.2) and a wider range of shape factors would be useful for practical purposes. The numerical model could then be used for reproducing the complex flow field during an anticipated flood over the misshaped beds of existing reservoirs (e.g. after the flushing operation). The results could be sustainable flood risk management in reservoirs, particularly those near urban areas, by effectively predicting the water levels and the

consequential fluvial processes. Moreover, a detailed sensitivity analysis of flow field to various influential parameters including hydraulic and numerical parameters could enrich this study field. Specifically, in reservoirs with an A1 flow pattern and a lower shape factor (SF) such as T7, the contribution of roughness in addition to the perturbation should be assessed to initiate the A1 flow pattern in a future study.

- 3D numerical modelling enables us to simulate the flow and sedimentation pattern with a resolution over the flow depth. Consequently, the effects of different measures on the flow pattern can be evaluated to direct sedimentation into preferential zones. Thus, the results of this paper can be applied to optimally design sand trap facilities or reservoirs for low-head power plants to increase or decrease the sedimentation. Regarding the prototype scale reservoirs, the shallow-flow condition emerges during the sediment flushing operation with full drawdown, and plays a significant role in removing deposited sediment from the reservoir. Different velocity distribution patterns may lead to different morphological processes in the reservoir. Therefore, 3D numerical models can be used to predict and manage shallow-flow behaviour under different scenarios to increase flushing efficiency. However, the coupled

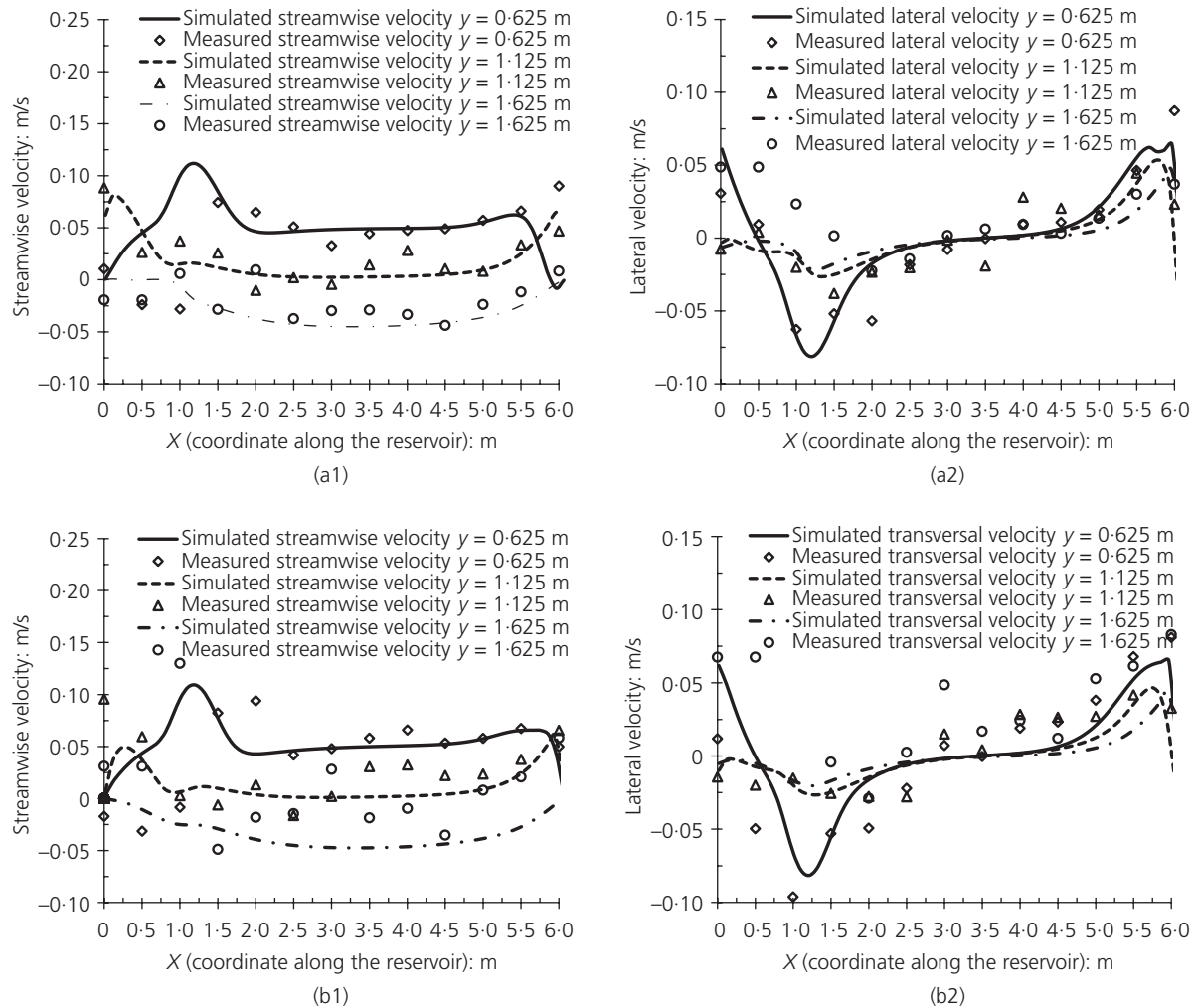


Figure 11. Left: the measured streamwise velocity over the flow depth using UVP against the simulated velocity for case T8 with flat bed at (a1) $z=0.045$ m; (b1) $z=0.155$ m; right: measured

lateral velocity over the flow depth using UVP against the simulated one at (a2) $z=0.045$ m; (b2) $z=0.155$ m

simulation of flow and sediment field that interact with the movable bed under unsteady flow conditions during a drawdown flushing is challenging; this problem should be numerically investigated using 3D numerical models for both physical and prototype-scale models. The results could provide a valuable perspective for upcoming sediment management measures and plans (e.g. free-flow flushing operations) in existing reservoirs.

REFERENCES

Adamson A, Stovin V and Bergdahl L (2003) Bed shear stress boundary condition for storage tank sedimentation. *Journal of Environmental Engineering, ASCE* **129**(7): 651–658.

Camnasio E, Ercicum S, Orsi E et al. (2013) Coupling between flow and sediment deposition in rectangular shallow reservoirs. *Journal of Hydraulic Research* **51**(5): 535–547.

Chiang TP, Sheu TWH and Wang SK (2000) Side wall effects on the structure of laminar flow over plane symmetric sudden expansion. *Computers & Fluids* **29**(5): 467–492.

Chu VH, Wu JH and Khayat RE (1991) Stability of transverse shear flows in shallow open channels. *Journal of Hydraulic Engineering, ASCE* **117**(10): 1370–1388.

Dehghani AA, Esmaeili T, Chang WY and Dehghani N (2012) 3D numerical simulation of local scouring under hydrographs. *Proceedings of the Institution of Civil Engineers – Water Management* **166**(3): 120–131, <http://dx.doi.org/10.1680/wama.11.00043>.

Dewals BJ, Kantoush SA, Ercicum S, Pirotton M and Schleiss AJ (2008) Experimental and numerical analysis of flow instabilities in rectangular shallow basins. *Environmental Fluid Mechanics* **8**(1): 31–54.

Dufresne M, Dewals B, Ercicum S, Archambeau P and Pirotton M (2011) Numerical investigation of flow patterns in

- rectangular shallow reservoirs. *Engineering Applications of Computational Fluid Mechanics* **5(2)**: 247–258.
- Dufresne M, Dewals B, Ericum S, Archambeau P and Piroton M (2012) Flow patterns and sediment deposition in rectangular shallow reservoirs. *Water and Environment Journal* **26(4)**: 504–510.
- Esmaili T, Sumi T, Chang WY and Vakili A (2013) Application of steady flows for simulating the local scour depth under time varying flows. In *Proceedings of the 12th International Symposium on River Sedimentation, Kyoto, Japan* (Fukuoka S, Nakagawa H, Sumi T and Zhang H (eds)). CRC Press, London, UK, pp. 905–912.
- Esmaili T, Sumi T, Kantoush SA and Schleiss AJ (2014a) Three dimensional numerical modelling of flow field in rectangular shallow reservoirs. In *Proceedings of the 7th River Flow Conference, Lausanne, Switzerland* (Schleiss AJ, De Cesare G, Franca MJ and Pfister M (eds)). CRC Press, London, UK, pp. 11–19.
- Esmaili T, Sumi T and Kantoush SA (2014b) Experimental and numerical study of flushing channel formation in shallow reservoirs. *Journal of Japan Society of Civil Engineers: Hydraulic Engineering* **70(4)**: 19–24.
- Fischer-Antze T, Stoesser T, Bates P and Olsen NRB (2001) 3D numerical modelling of open-channel flow with submerged vegetation. *Journal of Hydraulic Research* **39(3)**: 303–310.
- Fischer-Antze T, Olsen NRB and Gutknecht D (2008) Three-dimensional CFD modeling of morphological bed changes in the Danube River. *Water Resources Research* **44(9)**: 1–15.
- Frey P, Champagne JY, Morel R and Gay B (1993) Hydrodynamics fields and solid particle transport in a settling tank. *Journal of Hydraulic Research* **31(6)**: 736–776.
- Ghidaoui MS and Kolyshkin AA (1999) Linear stability of lateral motions in compound open channels. *Journal of Hydraulic Engineering, ASCE* **125(8)**: 871–880.
- Harb G, Haun S, Schneider J and Olsen NRB (2014) Numerical analysis of synthetic granulate deposition in a physical model study. *International Journal of Sediment Research* **29(1)**: 110–117.
- Haun S and Olsen NRB (2012a) Three-dimensional numerical modelling of the flushing process of the Kali Gandaki hydropower reservoir. *Lakes & Reservoirs: Research & Management* **17(1)**: 25–33.
- Haun S and Olsen NRB (2012b) Three-dimensional numerical modelling of reservoir flushing in a prototype scale. *International Journal of River Basin Management* **10(4)**: 341–349.
- Kantoush SA (2007) Symmetric or asymmetric flow patterns in shallow rectangular basins with sediment transport. In *Proceedings of 32nd IAHR Congress. IAHR, Venice, Italy*.
- Kantoush SA (2008) *Experimental Study on the Influence of the Geometry of Shallow Reservoirs on Flow Patterns and Sedimentation by Suspended Sediments*. PhD dissertation,  col  Polytechnique F d rale de Lausanne, Lausanne, Switzerland.
- Kantoush SA and Schleiss AJ (2009) Channel formation in large shallow reservoirs with different geometries during flushing. *Journal of Environmental Technology* **30(8)**: 855–863.
- Kantoush SA, Bollaert E and Schleiss AJ (2008a) Experimental and numerical modelling of sedimentation in a rectangular shallow basin. *International Journal of Sediment Research* **23(3)**: 212–232.
- Kantoush SA, De Cesare G, Boillat JL and Schleiss AJ (2008b) Flow field investigation in a rectangular shallow reservoir using UVP, LSPIV and numerical modelling. *Flow Measurement & Instrumentation* **19(3)**: 139–144.
- Kantoush SA, Sumi T and Schleiss AJ (2010) Geometry effect on flow and sediment deposition pattern in shallow basins. *Journal of Japan Society of Civil Engineers: Hydraulic Engineering* **54**: 133–138.
- Kantoush SA, Sumi T, Murasaki M and Schleiss AJ (2011a) LSPIV implementation for environmental flow in various laboratory and field cases. *Journal of Hydro-environment Research* **5(4)**: 263–276.
- Kantoush SA, Sumi T and Takemon Y (2011b) Lighten the load. *International Water Power & Dam Construction Magazine* **2011**, May: pp. 38–45.
- Kolyshkin AA and Ghidaoui MS (2003) Stability analysis of shallow wake flows. *Journal of Fluid Mechanics* **494**: 355–377.
- Lauder BE and Spalding DB (1972) *Lectures in Mathematical Models of Turbulence*. Academic Press, London, UK.
- Mariotti G, Falcini F, Geleynse N et al. (2013) Sediment eddy diffusivity in meandering turbulent jets: implications for levee formation at river mouths. *Journal of Geophysical Research: Earth Surface* **118(3)**: 1908–1920.
- Olsen NRB (2013) *A Three Dimensional Numerical Model for Simulation of Sediment Movement in Water Intakes with Multiblock Option*. Department of Hydraulic and Environmental Engineering, The Norwegian University of Science and Technology, Trondheim, Norway. See <http://folk.ntnu.no/nilsol/ssiiim/> (accessed 10/02/2014).
- Olsen NRB and Kjellesvig HM (1999) Three-dimensional numerical modelling of bed changes in a sand trap. *Journal of Hydraulic Research* **37(2)**: 189–198.
- Patankar SV (1980) *Numerical Heat Transfer and Fluid Flow*. McGraw-Hill, New York, NY, USA.
- Peltier Y, Ericum S, Archambeau P, Piroton M and Dewals B (2014a) Experimental investigation of meandering jets in shallow reservoirs. *Environmental Fluid Mechanics* **14(3)**: 699–710.
- Peltier Y, Ericum S, Archambeau P, Piroton M and Dewals B (2014b) Meandering jets in shallow rectangular reservoirs: pod analysis and identification of coherent structures. *Experiments in Fluids* **55(6)**: 1–16.
- Peltier Y, Ericum S, Archambeau P, Piroton M and Dewals B (2014c) Meandering jets in shallow rectangular reservoir. In *Proceedings of the 7th River Flow Conference, Lausanne,*

- Switzerland (Schleiss AJ, De Cesare G, Franca MJ and Pfister M (eds)). CRC Press, London, UK, pp. 21–29.
- Ruether N, Singh JM, Olsen NRB and Atkinson E (2005) 3-D computation of sediment transport at water intakes. *Proceedings of the Institution of Civil Engineers – Water Management* **158(1)**: 1–7, <http://dx.doi.org/10.1680/wama.2005.158.1.1>
- Schlichting H (1979) *Boundary Layer Theory*. McGraw-Hill, New York, NY, USA.
- Shapira M, Degani D and Weihs D (1990) Stability and existence of multiple solutions for viscous flow in suddenly enlarged channels. *Computers & Fluids* **18(3)**: 239–258.
- Stansby PK (2006) Limitations of depth-averaged modeling for shallow wakes. *Journal of Hydraulic Engineering* **132(7)**: 737–740.
- Stoesser T, Ruether N and Olsen NRB (2010) Calculation of primary and secondary flow and boundary shear stresses in a meandering channel. *Advances in Water Resources* **33(2)**: 158–170.
- Stovin VR and Saul AJ (1996) Efficiency prediction for storage chambers using computational fluid mechanics. *Water Science & Technology* **33(9)**: 163–170.
- Tritthart M and Gutknecht D (2007) 3-D computation of flood processes in sharp river bends. *Proceedings of the Institution of Civil Engineers – Water Management* **160(4)**: 233–247, <http://dx.doi.org/10.1680/wama.2007.160.4.233>
- Wilson CA, Stoesser T, Olsen NRB and Bates PD (2003) Application and validation of numerical codes in the prediction of compound channel flows. *Proceedings of the Institution of Civil Engineers – Water and Maritime Engineering* **156(2)**: 117–128, <http://dx.doi.org/10.1680/wame.2003.156.2.117>.
- Yuce MI and Chen D (2003) An experimental investigation of pollutant mixing and trapping in shallow coastal re-circulating flows. In *Proceedings of the International Symposium on Shallow Flows, Delft, Netherlands* (Jirka GH and Uijtewaal WS (eds)). Taylor & Francis Group, London, UK, pp. 413–420.

WHAT DO YOU THINK?

To discuss this paper, please email up to 500 words to the editor at journals@ice.org.uk. Your contribution will be forwarded to the author(s) for a reply and, if considered appropriate by the editorial panel, will be published as discussion in a future issue of the journal.

Proceedings journals rely entirely on contributions sent in by civil engineering professionals, academics and students. Papers should be 2000–5000 words long (briefing papers should be 1000–2000 words long), with adequate illustrations and references. You can submit your paper online via www.icevirtuallibrary.com/content/journals, where you will also find detailed author guidelines.